Available online at www.sciencedirect.com
ScienceDirect
Biochimica et Biophysica Acta 1777 (2008) 295–307
Biochimica et Biophysica Acta BBA
www.elsevier.com/locate/bbabio

# Pulse ENDOR and density functional theory on the peridinin triplet state involved in the photo-protective mechanism in the peridinin–chlorophyll *a*–protein from *Amphidinium carterae*☆

Marilena Di Valentin [a,*], Stefano Ceola [a], Giancarlo Agostini [b], Giorgio Mario Giacometti [c], Alexander Angerhofer [d], Orlando Crescenzi [e], Vincenzo Barone [e], Donatella Carbonera [a]

[a] *Dipartimento di Scienze Chimiche, Università di Padova, via Marzolo 1, 35131 Padova, Italy*
[b] *CNR, Istituto di Chimica Biomolecolare, Sezione di Padova, via Marzolo 1, 35131 Padova, Italy*
[c] *Dipartimento di Biologia, Università di Padova, viale G. Colombo 3, 35131 Padova, Italy*
[d] *Department of Chemistry, The University of Florida, Gainesville, Florida 32611-7200, USA*
[e] *Dipartimento di Chimica "Paolo Corradini", Università Federico II di Napoli, complesso universitario Monte S.Angelo, via Cintia, I-80126 Napoli, Italy*

Received 7 November 2007; received in revised form 21 December 2007; accepted 28 December 2007
Available online 17 January 2008

**Abstract**

The photoexcited triplet state of the carotenoid peridinin in the Peridinin–chlorophyll *a*–protein of the dinoflagellate *Amphidinium carterae* has been investigated by pulse EPR and pulse ENDOR spectroscopies at variable temperatures. This is the first time that the ENDOR spectra of a carotenoid triplet in a naturally occurring light-harvesting complex, populated by energy transfer from the chlorophyll *a* triplet state, have been reported. From the electron spin echo experiments we have obtained the information on the electron spin polarization dynamics and from Mims ENDOR experiments we have derived the triplet state hyperfine couplings of the α- and β-protons of the peridinin conjugated chain. Assignments of β-protons belonging to two different methyl groups, with $a_{iso}$=7.0 MHz and $a_{iso}$=10.6 MHz respectively, have been made by comparison with the values predicted from density functional theory. Calculations provide a complete picture of the triplet spin density on the peridinin molecule, showing that the triplet spins are delocalized over the whole π-conjugated system with an alternate pattern, which is lost in the central region of the polyene chain. The ENDOR investigation strongly supports the hypothesis of localization of the triplet state on one peridinin in each subcluster of the PCP complex, as proposed in [Di Valentin et al. Biochim. Biophys. Acta 1777 (2008) 186–195]. High spin density has been found specifically at the carbon atom at position 12 (see Fig. 1B), which for the peridinin involved in the photo-protective mechanism is in close contact with the water ligand to the chlorophyll *a* pigment. We suggest that this ligated water molecule, placed at the interface between the chlorophyll–peridinin pair, is functioning as a bridge in the triplet–triplet energy transfer between the two pigments.


*Keywords:* PCP; Carotenoid; Triplet state; Pulse EPR; Pulse ENDOR; DFT; Hyperfine couplings

## 1. Introduction

Carotenoids play an important role in the lives of plants and photosynthetic bacteria. They are present in light-harvesting and reaction center complexes performing two major functions: they act as light-harvesting pigments and as photoprotective agents. Their role as antenna pigments is fulfilled by absorbing light in the blue-green region where chlorophylls (Chl) and bacteriochlorophylls (BChl) absorb weakly and delivering excitation energy to these pigments by rapid singlet–singlet energy transfer. Carotenoids play the photoprotective role by virtue of their low-lying triplet states. They quench Chl and BChl triplet states, which can be populated under high light conditions, by triplet–triplet energy transfer [1]. In this way they prevent the formation of singlet oxygen, a harmful oxidizing agent. This

☆ This paper is dedicated to Professor Giovanni Giacometti in occasion of the start-up of the new EPR laboratory.

* Corresponding author. Tel.: +39 049 827 5139; fax: +39 049 827 5161.
*E-mail address:* marilena.divalentin@unipd.it (M. Di Valentin).

0005-2728/$ - see front matter © 2008 Elsevier B.V. All rights reserved.
doi:10.1016/j.bbabio.2007.12.003

photoprotective function is therefore essential for photosynthesis in an oxygen-containing environment.

The availability of the high-resolution X-ray structure of several light-harvesting complexes stimulated the theoretical and experimental investigation on the excitation transfer between carotenoids and (B)Chls involved in light-harvesting and photoprotection processes, on the basis of the detailed knowledge of the organization of these pigments. While most of the effort has been devoted to study singlet excitation transfer pathways in light-harvesting systems, there are still open questions regarding triplet excitation pathways, and the carotenoid triplet state photo-physics. In this context, time-resolved and pulse electron paramagnetic resonance (EPR) have proved to be powerful spectroscopic techniques in probing the carotenoid triplet species through their magnetic properties: zero-field splitting (ZFS) parameters, electron spin polarization (ESP) and time-evolution of the ESP. Carotenoid triplet states have been studied in bacterial reaction centers [2–4], in antenna complexes of different species [5,6] and even in artificial photosynthetic systems consisting of carotenoid polyenes covalently linked to porphyrin and chlorophyll derivatives [5,7–9]. The initial ESP of the carotenoid triplet is inherited from the (B)Chl donor, based on spin angular momentum conservation during triplet–triplet energy transfer [5,7,10,11]. For this reason the initial ESP is specific for each photosynthetic system depending exclusively on the relative geometrical arrangement of the donor–acceptor couple and therefore on the organization of the pigments in the protein, which is species-dependent. On the contrary, the time-evolution of the ESP leads to a final polarization pattern (*eaeaea*) which is common to all carotenoid triplet states in all the different photosynthetic systems [5,6]. This common feature has been interpreted in different ways: the initial ESP evolves to the final *eaeaea* polarization pattern because of the highly anisotropic decay of the three spin sublevels of the carotenoid triplet state to the singlet ground state, the anisotropy being an intrinsic feature of the carotenoid molecule [5]. Alternatively, conformational changes in the conjugated polyene chain occurring upon triplet excitation cause a change of the orbital angular momentum and as a consequence a change of the spin angular momentum through spin-orbit coupling. These phenomena produce an enhancement of the $T_1$–$S_0$ intersystem crossing, which itself is responsible for the time-evolution of the ESP. This latter hypothesis has been proposed for the 15-*cis*-spheroidene carotenoid bound to the reaction center from *Rhodobacter sphaeroides* 2.4.1.[2,4]. Carotenoids in antenna proteins are present in the all-*trans* configuration and the 15-*cis*-carotenoid is a unique feature of the reaction center together with its capability for rapid isomerization toward all-*trans* upon triplet excitation [12].

In a recent time-resolved EPR study, the concept of spin angular momentum conservation during triplet energy transfer was exploited to investigate the mechanism of photoprotection in the peridinin–chlorophyll *a*–protein (PCP) from *A. carterae* [13].

This water-soluble protein constitutes the peripheral light-harvesting complex of photosynthetic dinoflagellates and is characterized by a pigment stoichiometry of 8 peridinins to

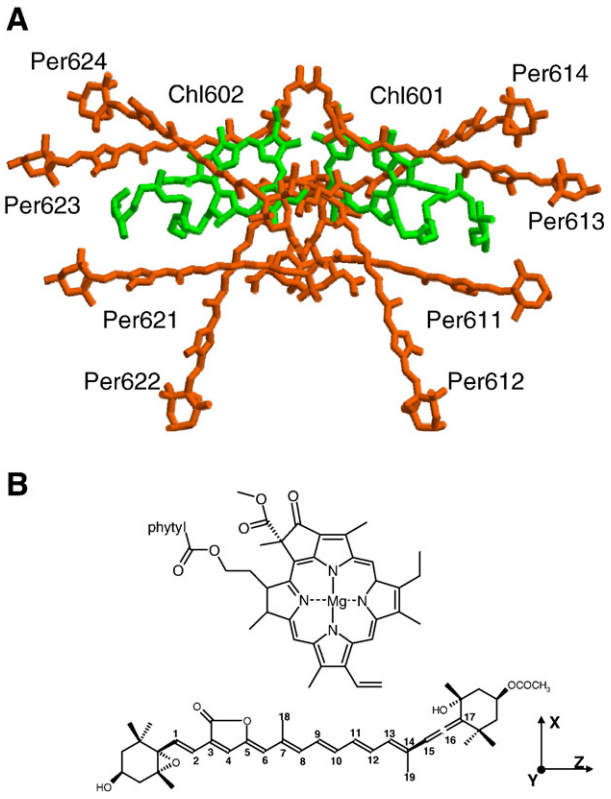


Fig. 1. (A) Structure of the pigments associated with the monomeric basic unit of the PCP complex from *A. carterae*. The coordinates are taken from PDB code 1 PPR deposited in the Brookhaven Protein Data Bank by Hofmann et al. [14]. The protein scaffold has been omitted for clarity. (B) Molecular structures of chlorophyll *a* and peridinin. The numbering scheme and the orientation of the ZFS tensor axes according to [35] are reported for peridinin.

2 Chl *a* molecules (see Fig. 1A). A high carotenoid content and the presence of peridinin (Per), an unusual light-harvesting carotenoid (the molecular structure is reported in Fig. 1B) are distinctive characteristics of the PCP antenna protein. Peridinin is an asymmetric and highly substituted carotenoid with a $C_{37}$ carbon skeleton (rather than $C_{40}$ as in most carotenoids) together with a lactone ring, an allene moiety in conjugation with the π-electron system and two terminal β-rings with epoxy and acetate substituents. The structure of PCP from *Amphidinium carterae* (*A. carterae*) has been resolved at 2.0 Å resolution [14]. It shows a trimeric subunit arrangement, in each subunit the pigments are organized in two pseudo-identical domains of four peridinins in van der Waals contact (3.3 to 3.8 Å) with the tetrapyrrole ring of one Chl *a* molecule. Peridinins are in an almost extended all-*trans* configuration and show small distorsions from their average geometry, which derive from the interaction with the surrounding protein. Distances among peridinins within a single domain range from 4 to 11 Å.

In the isolated form of PCP, the Chl *a* pigments, once excited, cannot transfer their energy on to other antenna complexes and de-excitation mainly proceeds through fluorescence or intersystem crossing and triplet formation. The lifetime of the Chl *a* triplet state is of the order of 20 ns, within this time a triplet state is formed on one of the circumferential peridinins and

decays through radiationless intersystem crossing channels with a lifetime of 10 μs at room temperature [15].

In our recent report on the triplet excitation pathways in the PCP antenna, we simulated the initial ESP pattern of the TR-EPR spectrum of the peridinin triplet state [13] as inherited from the Chl *a* triplet state, in the framework of spin conservation. Starting from the relative populations of the chlorophyll triplet state and taking the relative positions among Chls and peridinins into account, as determined by the X-ray structure of PCP, we calculated the expected triplet state polarization of any peridinin in the complex. Comparison with the experimental data allowed us to suggest a specific path for triplet energy transfer in this protein.

The time-resolved study demonstrated that the chlorophyll–peridinin pair directly involved in the triplet–triplet energy transfer coincides with the one having the shortest center to center distance (Chl601/602 and Per614/624 according to the nomenclature used in [13] and reported in Fig. 1A). This particular pair has a water molecule in a bridging position which is coordinated to the central Mg atom of the Chl. Furthermore, the EPR results support the concept of localization of the triplet state mainly in one specific peridinin in each of the two pigment subclusters in a wide temperature range up to physiological temperatures.

It is interesting to seek a correlation between the specific pairs Chl601(602)–Per614(624) identified as the active ones in the photo-protective mechanism, and the structural requirements for efficient triplet–triplet energy transfer as indicated by the X-ray structure. The triplet–triplet energy transfer process is based on the Dexter mechanism and the efficiency of the transfer depends on the overlap of the wavefunctions of donor and acceptor [16,17]. Detailed knowledge of the electronic structure of the triplet state of the molecules involved in the transfer is necessary in order to investigate this issue.

Further insight into the problem derives from the extension of the spectroscopic study of the peridinin triplet state in PCP using pulse electron-nuclear double resonance (ENDOR) spectroscopy. Pulse ENDOR opens the possibility to resolve the electron-nuclear hyperfine structure of short-lived species having lifetimes in the microsecond range.

While a large body of ENDOR experiments has been performed on the β-carotene cation radical in photosystem II [18] and on different carotenoids radicals in organic solvents or solid supports [19–21], using both pulse and continuous-wave ENDOR methods, no information is available on the hyperfine coupling constants (hfcs) for the triplet state of any carotenoid present in photosynthetic proteins.

Triplet state ENDOR, using time-resolved or pulse methods, has been successfully applied to porphyrin and (B)Chl model systems [22–24], to the primary donor $^{T}$P680 in plant photosystem II [25,26] and to the primary donor $^{T}$P865 of the photosynthetic bacterium *R. sphaeroides* [27]. Therefore, while a complete picture of the triplet state hfcs is available for porphyrin-based molecule, the information is still lacking for the carotenoid molecules, which represent together with (B)Chls the essential pigments for the light-reactions of oxygenic photosynthesis.

In this paper we report the first detailed pulse EPR/ENDOR investigation on the peridinin triplet state, formed by triplet–triplet energy transfer from the Chl *a* triplet donor in PCP from *A. carterae*. Preliminary ENDOR experiments on the peridinin triplet state in the PCP complex from a different dinoflagellate species, *Heterocapsa pygmaea*, are reported in [28]. The combined application of the pulse EPR and pulse ENDOR techniques, at variable delay-after-flash (DAF) periods between the laser flash, used to photo-excite the triplet species, and the microwave pulse sequence, allows us to discuss in detail the ESP dynamics and to obtain the hyperfine coupling information on the peridinin triplet state.

In this contribution we compare the proton hfcs obtained from ENDOR experiments with those predicted from density functional theory (DFT), with the aim of determining the triplet spin density on the conjugated chain of the peridinin carotenoid and correlate it with the structural requirements for efficient triplet–triplet energy transfer. These experiments should open the door to further triplet ENDOR studies on different carotenoids in light-harvesting complexes of bacteria and higher plants.

## 2. Materials and methods

### 2.1. Sample preparation

*PCP* proteins, extracted and purified according to Sharples et al. [29], were kindly supplied by RG. Hiller. Sample concentrations were ≈1 mg/ml. Oxygen was removed from the samples by flushing argon in the EPR tube before freezing, residual oxygen was removed using glucose/glucose oxidase. Glycerol, previously degassed by several cycles of freezing and pumping, was added (60%v/v) to obtain a transparent matrix.

### 2.2. Pulse EPR and ENDOR measurements

Pulse EPR and ENDOR were performed on a Bruker Elexsys E580 pulse EPR spectrometer equipped with a Bruker ENDOR accessory (E560D-P) and a radio frequency (RF) amplifier (AR751 — 150 W). Laser excitation at 532nm (10 mJ per pulse and repetition rate of 10 Hz) was provided by the second harmonic of a Nd:YAG laser (Quantel Brilliant) in the optically transparent dielectric ring ENDOR resonator (EN4118X-MD4). After pulsed laser excitation, the EPR and ENDOR signals were directly detected and have a non-derivative shape.

The temperature was controlled with a helium cryostat (Oxford CF935) driven by a temperature controller (Oxford ITC503).

Field-swept electron spin echo (ESE) spectra were recorded using a 2-pulse (flash-DAF-π/2-τ-π-τ-echo) ESE sequence for three different values of DAF (50 ns, 18 μs, 40 μs) between the laser flash and the first microwave (MW) pulse. ESE-detected kinetics at the triplet canonical orientations were recorded using a 2-pulse (flash-DAF-π/2-τ-π-τ-echo) ESE sequence after a variable DAF (500 ns step) between the laser flash and the first MW pulse. The π/2-pulse was of 16 ns and the delay τ was set at 200 ns for the field-swept ESE experiment and to 120 ns for the ESE-detected kinetics.

Mims ENDOR experiments were recorded using the MW pulse sequence flash-DAF-π/2-τ-π/2-T-π/2, with 16 ns pulse duration, in conjunction with an RF pulse of 3 μs duration, starting 0.3 μs after the second MW pulse. The DAF was 50 ns, the delay τ was variable, and the time T was 3.8 μs to accommodate the RF pulse. Mims ENDOR spectra were recorded at different τ values (from 160 ns to 240 ns) and added together to eliminate τ dependent blind spots. Pulse ENDOR spectra were accumulated for ≈15 h.

### 2.3. EPR spectral analysis

A program written in MatLab® was employed to analyze the pulse EPR spectra. The program calculates both the line shape and the time profile of the spin-polarized triplet EPR spectrum. The program is based on a spin Hamiltonian

in which only the Zeeman and magnetic dipole–dipole interaction (ZFS parameters $D$ and $E$) are explicitly taken into account to calculate the line shape of the spectrum for an ensemble of randomly oriented molecules.

The time-evolution of the ESE-detected spectrum has been calculated in terms of the photo-excited triplet state dynamics, as previously described [30]. The echo decay reflects the time development of the population difference of the two spin sublevels connected, i.e.:

$$I(t) = [\pm A_1 \exp(-k_1 t)] - [\pm A_0 \exp(-k_0 t)]$$

where $A_1$ and $A_0$ are the initial relative populations of $T_{+1}/T_{-1}$ and $T_0$, respectively, and $k_1$ and $k_0$ are the corresponding decay rates to the singlet ground state (signs in the biexponential depend on the absorption or emissive nature of the transition).

### 2.4. Quantum mechanical computations

Quantum mechanical computations have been performed by the G03 package [31] using the B3LYP hybrid functional; geometries have been optimized at the 6–31G(d) level [32], whereas hfc constants have been computed by the purposely tailored EPR-II basis set [33,34]. The axes of dipolar couplings are oriented along the ZFS axes as determined experimentally.

## 3. Results

### 3.1. EPR

Fig. 2 depicts the field-swept ESE spectrum of the photo-excited triplet state of peridinin in PCP from *A. carterae,* recorded immediately after the laser flash (DAF of 50 ns) at 20 K. The spectrum is in agreement with previous time-resolved EPR results, showing the same *eaeaea* spin polarization pattern and ZFS parameters ($|D|=449.7\times10^{-4}$ cm$^{-1}$, $|E|=43.9\times10^{-4}$ cm$^{-1}$), and can be therefore assigned to the peridinin triplet

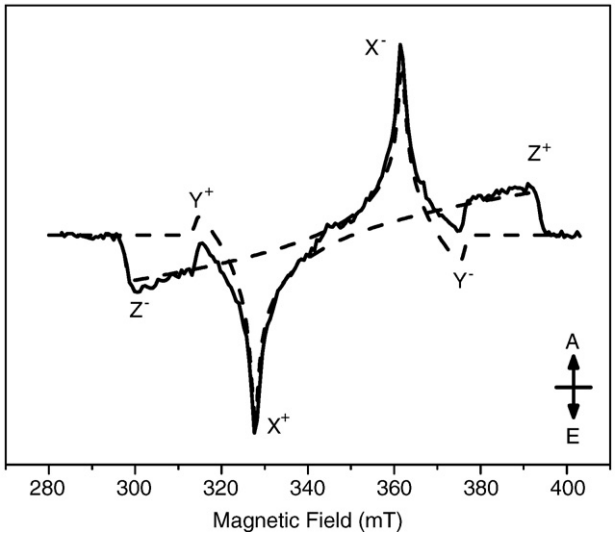


Fig. 2. Field-swept ESE spectrum of PCP from *A. carterae* at $T=20$ K, together with the powder simulations (dashed lines) for the $m_S=+1$ to the $m_S=0$ transitions (index +) and the $m_S=0$ to the $m_S=-1$ transitions (index −). Parameters used for the simulation are reported in Table 1. *X*, *Y*, *Z* ZFS tensor canonical orientations are indicated. Order of energy for zero-field triplet sublevels: $|Z|>|Y|>|X|$. A = absorption, E = emission. For experimental conditions see Materials and methods.

Table 1
Parameters of peridinin triplet state

| $\|D\|$ ($10^{-4}$ cm$^{-1}$) | $\|E\|$ ($10^{-4}$ cm$^{-1}$) | $P_X$: $P_Y$: $P_Z$ | $k_X$: $k_Y$: $k_Z$ (μs$^{-1}$) |
|---|---|---|---|
| 449.7 | 43.9 | 0.18: 0.37: 0.45 | 0.15: 0.03: 0.09 |

This table reports the values of the relative population rates $P_X$, $P_Y$ and $P_Z$ of the triplet sublevels together with the ZFS parameters $|D|$ and $|E|$, derived from simulation of the field-swept ESE spectrum. The table reports also the decay constants $k_X$, $k_Y$ and $k_Z$ of the triplet sublevels obtained from the analysis of the time-evolution of the ESE-spectrum, using the model described in the Materials and methods. The order of the ZFS energy levels is: $Z^2>Y^2>X^2$.

[13]. The polarization pattern is inherited from the Chl *a* triplet donor in the triplet–triplet energy transfer mechanism as demonstrated in [13]. No difference in spectral profiles is observed when comparing the time-resolved and the echo-detected spectra, proving that the spin–spin relaxation time is not orientation dependent and sufficiently longer than the τ value of 200 ns used in the pulse EPR experiments.

In Fig. 2 the experimental spectrum is superimposed with the spectral simulation (parameters are reported in Table 1). The dashed traces correspond to the simulated powder pattern for the $m_S=0$ to $m_S=+1$ transition ($X^+$,$Y^+$,$Z^+$) and for the $m_S=0$ to $m_S=-1$ transition ($X^-$,$Y^-$,$Z^-$). The order of the ZFS energy levels is: $Z^2>Y^2>X^2$. The corresponding ZFS axes of the peridinin triplet state have been chosen analogously to those determined for β-carotene in crystals [35,36]: the long axis is the *Z* axis, the *X* axis is along the C–H bonds in the conjugated chain and the *Y* direction is perpendicular to the conjugated *XZ* molecular plane (see Fig. 1B).

### 3.2. ENDOR

Triplet ENDOR experiments, performed at the canonical magnetic field positions in the EPR spectrum, permit measurement of the $A_{ii}$ hfc tensor components of protons in the reference frame of the ZFS tensor, yielding single-crystal-like spectra.

The triplet spin energy levels for the *X* orientation, including first-order hyperfine interaction with one proton $A_{XX}$, for $D<0$ as expected for a carotenoid molecule characterized by a long axis, are shown in Fig. 3A. For each EPR transition, there are two ENDOR resonance frequencies at:

$\nu_{ENDOR}(0)=\nu_H$
$\nu_{ENDOR}(1)=\nu_H-A_{XX}$ if $A_{XX}>0$ or $\nu_{ENDOR}(1)=\nu_H+A_{XX}$ if $A_{XX}<0$
corresponding to the $X^+$ EPR transition or
$\nu_{ENDOR}(0)=\nu_H$
$\nu_{ENDOR}(-1)=\nu_H+A_{XX}$ if $A_{XX}>0$ or $\nu_{ENDOR}(-1)=\nu_H-A_{XX}$ if $A_{XX}<0$
corresponding to the $X^-$ EPR transition.

The ENDOR transitions corresponding to the $\Delta m_S=\pm 1$ EPR transitions in the low-field and high-field spectra are reflected on opposite sides of the transition at $\nu_H$. For the $X^+$ transition, depending on the sign of $A_{XX}$, the ENDOR lines occur on the low (if $A_{XX}>0$) or high (if $A_{XX}<0$) frequency side. An opposite

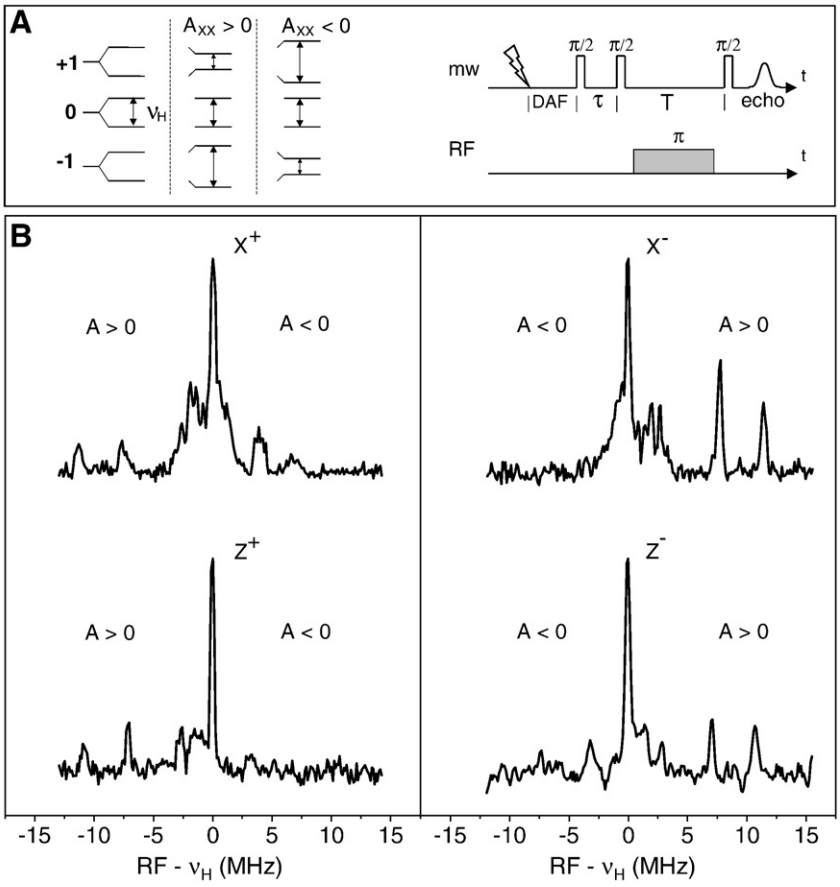


Fig. 3. (A) Left: spin energy levels of a triplet state showing positive and negative hyperfine interaction with one nucleus with spin $I=1/2$ for the field parallel to the $X$ ZFS tensor axis. Right: pulse scheme for the Mims ENDOR experiment for photoexcited triplet states. (B) Pulse Mims ENDOR spectra of PCP from *A. carterae* for the $X$ and $Z$ EPR field positions (indicated in Fig. 2) at $T=20$ K. The ENDOR spectra for the $X^+$ and $Z^-$ EPR transitions are in emission but has been inverted for better comparison. The frequency scale gives the deviation from the $\nu_H$ and the hfcs correspond to the frequency shift between the corresponding ENDOR line and the $\nu_H$. Expected frequency ranges for ENDOR lines corresponding to $A>0$ and $A<0$ are shown. For experimental conditions see Materials and methods.

situation is encountered for the $X^-$ transition. Therefore if the sign of the ZFS parameter $D$ is known, as for the peridinin molecule, the sign of the hfcs can be directly derived from the spectral position corresponding to the low/high-field lines.

The experimental Mims ENDOR spectra of the photoexcited triplet state of peridinin in PCP from *A. carterae*, at the $X^+$ and $X^-$ EPR field positions, obtained at 20 K, are reported in Fig. 3B. The ENDOR spectrum for the $X^+$ transition is spin-polarized in emission as the corresponding EPR transition, but it has been inverted in Fig. 3B for better comparison with the high-field counterpart. The frequency scale in this figure is plotted as deviation from $\nu_H$ and the hfcs correspond to the frequency shift between the corresponding ENDOR line and the $\nu_H$. Based on the scheme reported in Fig. 3A ENDOR lines have been labelled in terms of positive or negative hfcs. Both spectra show a strong line at $\nu_H$ and additional partially resolved lines are present in the vicinity of the free proton line corresponding to positive hfcs $A_{XX}\leq 2.7$ MHz. Only lines corresponding to positive hfcs $A_{XX}$ are reflected on opposite sides of the transition $\nu_H$ in the low and high-field spectra. The mirror images of the two transition at $\nu_H+3.6$ MHz and $\nu_H+6.9$ MHz in the low-field $X^+$ spectrum, corresponding to negative hyperfine couplings, have not been detected in the high-field $X^-$ spectrum. Their absence can be explained considering that they would appear in the RF low-frequency region where there is no hyperfine-enhancement of the applied RF field [37]. Therefore all lines, even those missing the counterpart, can be assigned to protons.

Pulse ENDOR spectra of the peridinin triplet state in PCP were also measured for the other canonical orientations where the static magnetic field is parallel to the zero-field axes $Y$ and $Z$. The comparison between the ENDOR spectra for the $X^+$ and $Z^+$ transitions and for the $X^-$ and $Z^-$ transitions are reported in Fig. 3B. The ENDOR spectra performed at the $Z^+$ and $Z^-$ magnetic field positions are mirror images with respect to the proton Zeeman frequency and both show the same ENDOR transitions. The spectrum for the $Z^-$ is polarized in emission as the corresponding EPR transition, but has been inverted in Fig. 3B for better comparison with the high-field counterpart.

The ENDOR spectra for the $Y$ EPR transitions is only showing an unstructured line at $\nu_H$ and for this reason is not shown. For the $Y$ orientations the pulse EPR spectrum, at short DAF, is showing very small signal intensity, precluding the possibility to obtain pulse ENDOR spectra corresponding to the initial polarization, as produced by triplet–triplet energy transfer, for these orientations.

Table 2
Proton hyperfine couplings for the peridinin triplet state as derived from pulse ENDOR experiments

| $A_{XX}$ (MHz) | $A_{YY}$ (MHz) | $A_{ZZ}$ (MHz) |
|---|---|---|
| 11.4 | 9.8 | 10.7 |
| 7.6 | 6.2 | 7.1 |
| 2.7 | 1.2 | 2.9 |
| 1.9 | −0.9 | 1.5 |
| 1.4 | −4.1 | 0.8 |
| 0.8 | −6.9 | −3.3 |
| −0.9 | | |
| −3.6 | | |
| −6.9 | | |

This table reports the experimental values of the proton hyperfine tensor components in the ZFS axes system of the peridinin molecule. The ZFS reference frame is reported in Fig. 1B.

When comparing the ENDOR spectra respectively at the $X^+$ and $Z^+$ field positions and at the $X^-$ and $Z^-$ field positions, some clear superpositions between spectra can be recognized. The two narrow ENDOR transitions, appearing on the low RF side from $\nu_H$ in the $X^+$ and $Z^+$ spectra and on the high RF side from $\nu_H$ in the $X^-$ and $Z^-$ spectra, are almost coincident and correspond to positive hfcs: $A_{XX}$=11.4 MHz /$A_{ZZ}$=10.7 MHz and $A_{XX}$=7.6 MHz /$A_{ZZ}$=7.1 MHz. Based on their small anisotropy, these positive couplings are assigned to two sets of equivalent protons belonging to rotating methyl groups. The two methyl groups at positions 18 and 19 in the molecular structure (see Fig. 1B), positioned in the conjugated region of the polyene chain, are expected to show up with significant positive hfcs in the ENDOR spectra in agreement with the experimental findings. The averaged hfc tensor of three equivalent rotating methyl protons should be axially symmetric with an anisotropy less than 10% of the respective isotropic hcfs [38]. Furthermore the largest value is expected in the C–$CH_3$ bond direction, which should correspond to the ZFS $X$ axis canonical orientation. Indeed, experimental $A_{XX}$ for both methyl groups are found to be the largest couplings [38].

Few negative hfc components, that are highly anisotropic as proven by their different spectral position in the ENDOR spectra for $X$ and $Z$ canonical transitions, have been detected. It has been previously demonstrated for carotene radicals in frozen solution or solid supports that the lines corresponding to α-protons broaden and become undetectable in powder ENDOR spectra because of their large anisotropic component [18,21].

All the spectra at $X$ and $Z$ EPR field positions show partially resolved lines in the vicinity of the proton Zeeman frequency corresponding to positive hfcs $A_{XX} \leq 2.7$ MHz or $A_{ZZ} \leq 2.9$ MHz. No methyl protons can contribute to these positive couplings since apart from the methyl 18 and 19, already assigned to the large positive couplings, all the other methyl groups are located in the two terminal unconjugated β-rings. These small positive hfcs components belong to α-protons and become detectable, despite the large anisotropy expected for these type of protons, because of the sensitivity of the Mims ENDOR experiment for detecting ENDOR lines corresponding to small hfcs [37].

All hf tensor components, measured in the $X$ and $Z$ directions of the ZFS reference frame, are summarized in Table 2. The ZFS and hfc tensor axes for α-protons and for the two sets of rotating methyl protons can be considered collinear within ±10°.

The temperature dependence of the ENDOR spectrum corresponding to the $X^-$ EPR transitions is reported in Fig. 4. Mims ENDOR measurements were carried out at 5–150 K. In this temperature range, the spectra did not show any significant line shape variation which would reveal variations in the rotational dynamics of the methyl group. This implies very rapid rotation of the methyl groups, in the EPR time-scale, even at 5 K. Rotation down to cryogenic temperatures was already observed in ENDOR experiments of carotenoid radicals [18,21] and also in (B)Chl triplet states [25–27]. The same invariance with the temperature has been found also for the ENDOR lines corresponding to the $X^+$, $Z^-$ and $Z^+$ EPR magnetic field positions (data not shown).

### 3.3. ESE-detected kinetics

We have also investigated the kinetics of population and decay of the triplet spin sublevels by monitoring the echo intensity as a function of DAF, the delay of the microwave pulse sequence with respect to the laser flash. While kinetic measurements in time-resolved EPR are hampered by the presence of microwave-induced transition probabilities, ESE spectroscopy does not suffer of this complication since in this technique there is no microwave field present in the period between the photogeneration of the triplet state and its detection. Fig. 5A shows the ESE-detected EPR spectra of PCP from *A. carterae* at different DAF (50 ns, 18 μs, 40 μs) at 20 K.

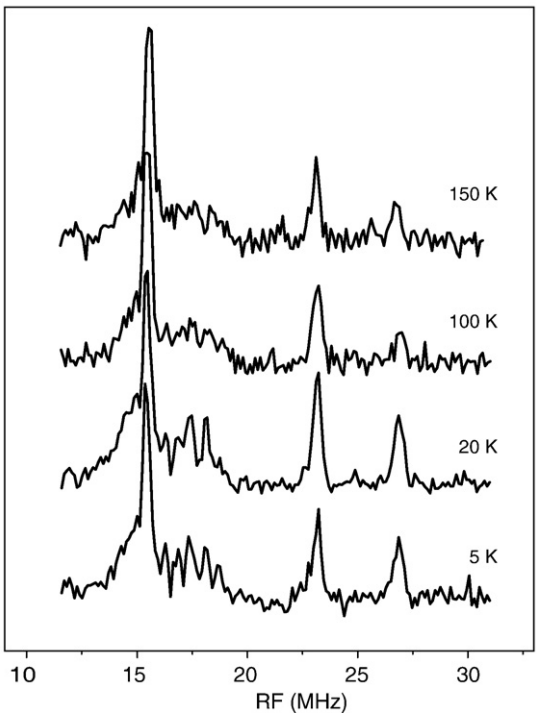


Fig. 4. The temperature dependence (5 K–150 K) of the pulse Mims ENDOR spectra of PCP from *A. carterae* at the $X^-$ EPR field position.

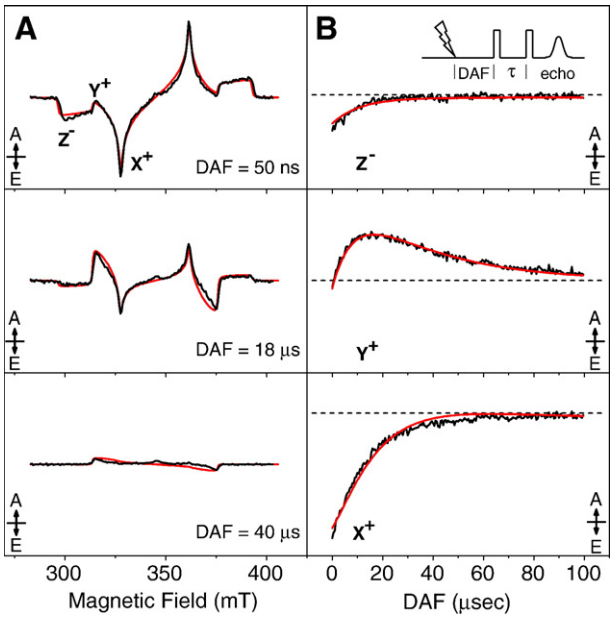


Fig. 5. (A) Field-swept ESE spectrum of PCP from *A. carterae*, at $T=20$ K, at different DAF (black lines), from top to bottom at 50 ns, 18 µs and 40 µs, and the corresponding powder simulations (red lines). (B) ESE-detected kinetics, at $T=20$ K, at the low-field canonical fields $Z^-$, $Y^+$, $X^+$ (black lines) and the corresponding simulations (red lines). Simulations are based on the kinetic model described in the Materials and methods section and the parameters are reported in Table 1. A=absorption, E=emission. For experimental conditions see Materials and methods. Inset: Pulse scheme of the ESE experiment for photoexcited triplet states.

The overall ESE-detected kinetics in function of DAF at the low-field canonical orientations of the ZFS tensor ($Z^-$, $Y^+$, $X^+$) are reported in Fig. 5B. No variation of the ZFS parameters, which have been attributed to the peridinin triplet state in agreement with previous ODMR and TR-EPR investigations [13,39], are occurring in the time course, proving that the same triplet species has been detected in the overall time-evolution of the spectrum. In contrast, the spin polarization varies in time, showing a polarization inversion at the *Y* canonical resonance, which is clearly visible both in the time-evolution of the EPR spectrum and in the time-trace corresponding to the $Y^+$ field position. The ESE-detected kinetics do not show any temperature dependence in the range 5 K–100 K (data not shown), higher temperature checks were precluded by the echo intensity reduction induced by fast spin–spin relaxation.

The time-evolution of the EPR spectrum was calculated in terms of the photo-excited triplet state dynamics [30], assuming that the echo decay reflects the decay kinetics of the triplet sublevel populations. This assumption can be considered valid since no spin–lattice relaxation effect was detected in the temperature range investigated. The delay τ between the two microwave pulses was adjusted to a minimum value in order to avoid also spin–spin relaxation effects.

Fig. 5A shows the simulations of the time-dependence of the entire spectrum for discrete values of DAF, as selected experimentally, superimposed to the corresponding experimental spectra. The comparison between the experimental and calculated transient traces at the low-field canonical transitions are reported in Fig. 5B. Since the kinetics at the *X* and *Y* canonical fields are strongly mixed because of the superposition of several transitions, the transient traces detected at the canonical transitions were not simulated in the simplified view of single canonical transitions. The calculated time-traces were extracted, in correspondence of the *X*, *Y* and *Z* spectral turning-points, from a bidimensional simulation of the EPR spectrum of the peridinin triplet state as a function of both the static magnetic field and delay from the laser pulse. In Table 1 we summarize the relative populating rates and decay rates for the peridinin triplet levels. The time-dependent changes of the spin polarization, including the spin polarization inversion detected at the *Y* canonical transitions, are satisfactorily reproduced by simulations, proving that the phenomenon we are detecting is the strongly anisotropic decay of the three spin sublevels of the peridinin triplet state to the ground singlet state.

Further evidence comes from the comparison between the Mims ENDOR spectra of the photoexcited peridinin triplet state recorded at different delay times between the laser flash and the ENDOR pulse sequence. Fig. 6A shows the ENDOR spectra corresponding to the $X^-$ canonical transition for the minimum set-up delay (50 ns) and for a DAF of 18 µs ($T=20$ K). The choice of the 18 µs delay time comes from inspection of the transient trace recorded at the canonical fields using the same pulse sequence as in the Mims ENDOR experiment but without the RF pulse (data not shown). Maximum inversion of the spin polarization at the *Y* canonical transition occurs at DAF=18 µs, and contemporarily at this delay time the spin polarization at the *X* canonical transition is not decayed completely allowing detection of this component. The comparison of the initial ENDOR spectrum for the $X^-$ EPR transition with

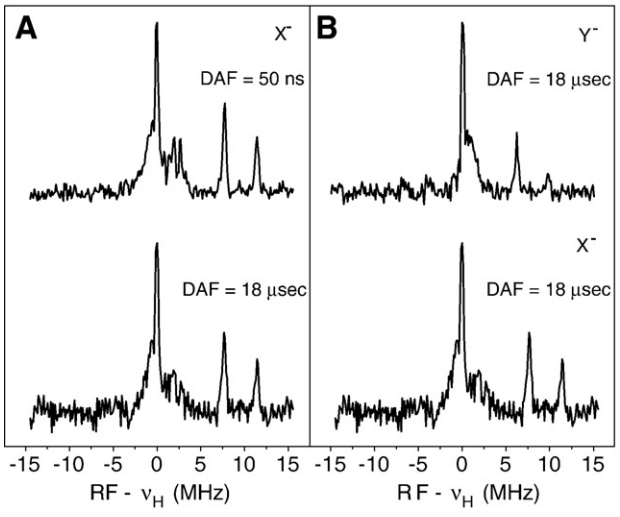


Fig. 6. (A) Pulse Mims ENDOR spectra of PCP from *A. carterae* at $T=20$ K for the $X^-$ EPR field positions at different delay times after the laser flash: DAF=50 ns for the upper spectrum, DAF=18 µs for the lower spectrum. (B) Pulse Mims ENDOR spectra of PCP from *A. carterae* at $T=20$ K and DAF=18 µs for the $Y^-$ and $X^-$ EPR field positions. The frequency scale gives the deviation from the $\nu_H$ and the hfcs correspond to the frequency shift between the corresponding ENDOR line and the $\nu_H$. Inset: Pulse scheme for the Mims ENDOR experiment for photoexcited triplet state.

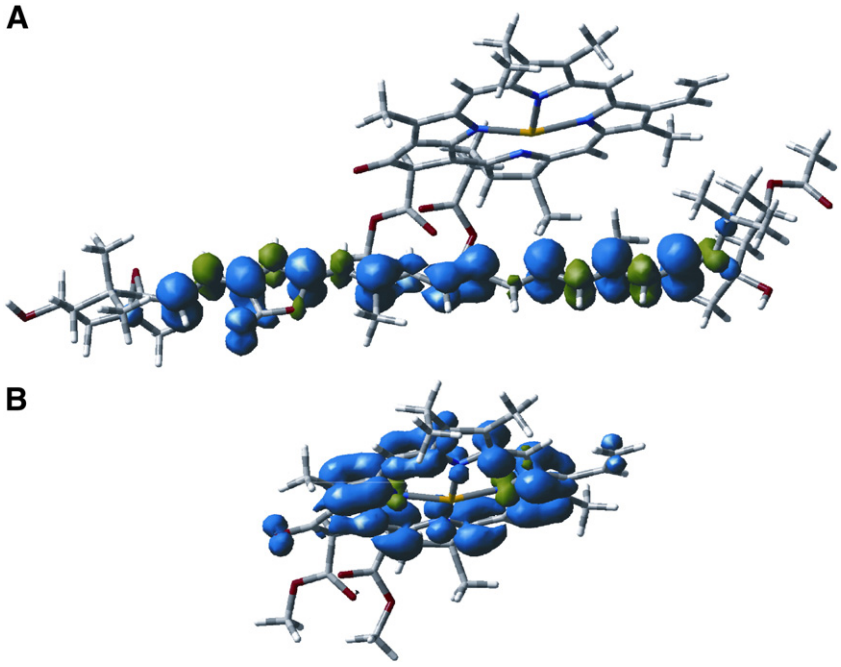


Fig. 7. Computed spin densities (B3LYP/EPR-II) for the triplet state localized on Per614 (panel A) and for the triplet on Chl601 (panel B); the peridinin moiety is not shown for the sake of clarity.

the one obtained in correspondence of maximum spin polarization inversion (see Fig. 6A) is not showing any spectral variation in terms of ENDOR line shifts, appearance or disappearance of lines. The invariance in time of the detected triplet hfcs is important evidence that only one triplet species, which we have identified with Per614(624) in a recent manuscript [13], is detected in the overall time course of the EPR experiment.

As already pointed out, the pulse EPR spectrum, at short DAF, is showing very small signal intensity at the *Y* canonical transition, precluding the possibility to obtain pulse ENDOR spectra corresponding to the initial polarization. The spin polarization inversion is accompanied by an increase in signal intensity for the *Y* transition allowing detection of the ENDOR at delay times corresponding to maximum spin polarization inversion. Fig. 6B shows the ENDOR spectra for the $\bar{Y}$ and $\bar{X}$ EPR transitions, at 20 K for a DAF of 18 μs. The frequency scale is plotted as deviation from $\nu_H$ for a direct comparison of the spectral lines at the two canonical positions.

As in the previous comparison between the ENDOR spectra at the $\bar{X}$ and $\bar{Z}$ EPR field positions (see Fig. 3B), the two narrow ENDOR transitions, appearing at high RF frequencies in the spectra reported in Fig. 6B, correspond to positive hfcs and are characterized by small shifts in spectral position: $A_{XX}$=11.4 MHz / $A_{YY}$=9.8 MHz and $A_{XX}$=7.6 MHz /$A_{YY}$=6.2 MHz. As stated before, based on their small anisotropy, these positive hfcs are assigned to protons belonging to rotating methyl groups, at position 18 and 19 in the molecular structure (see Fig. 1B). All the three hyperfine tensor components in the ZFS tensor frame, for both methyl groups, have been determined from the ENDOR spectra shown in Figs. 3B and 6B. The corresponding values are reported in Table 2. Based on the approximate collinearity between the ZFS and hfc tensor principal axes, the hfc components measured in the ZFS frame can be considered the principal components of the proton hyperfine tensors. For this reason, the isotropic hfc constants for the two rotating methyl groups can be directly derived from the set of measured hfc components: $a_{iso}$=7.0 MHz and $a_{iso}$=10.6 MHz respectively.

### 3.4. Quantum mechanical computations

In order to gain more detailed information on the assignment of the observed experimental signals, and to get insight into the electronic features of the peridinin–chlorophyll system, we resorted to quantum mechanical computations of geometries and of spectroscopic parameters, using theory levels that have been validated in a number of studies [40]. We have performed several geometry optimizations of the peridinin molecule, but in the following we will discuss only the results issuing from optimization of hydrogen atoms, methyl groups, and allene moiety, while freezing all the other atoms in the positions found in the X-ray study for Per614(624) [14]. As a matter of fact, while backbone parameters issuing from X-ray diffraction and DFT geometry optimizations are comparable, this is not the case for the C–C bond lengths connecting methyl groups to the main chain (ca. 1.56 vs. 1.50 Å) and for the allenic moiety (1.39, 1.35 Å vs. 1.32, 1.31 Å). Since experimental values are far from accepted standards, whereas optimized ones are quite reasonable, we prefer to adopt the latter set. At the same time, hydrogen atoms are not available from the X-ray study and also in this case we resorted to optimized bond lengths.

Computations carried out along these lines on the whole chlorophyll–peridinin complex (Chl601–Per614) led to the identification of two low-lying triplet states localized respectively on the chlorophyll and the peridinin moiety: the corresponding spin

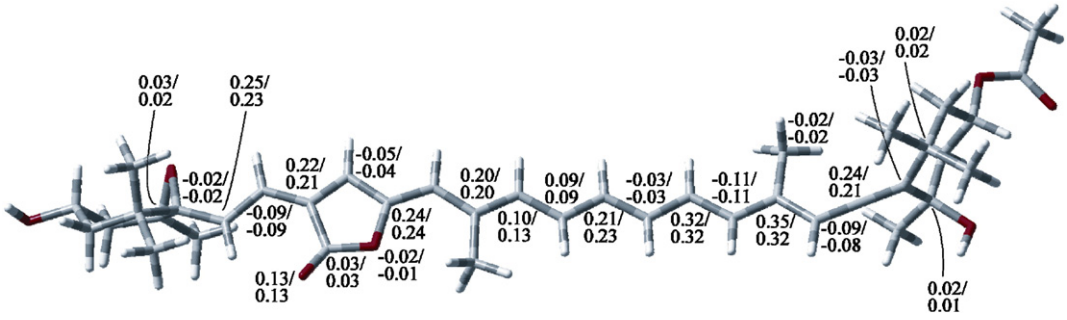


Fig. 8. Mulliken spin densities computed at the B3LYP/EPR-II level for the triplet state of Per614(624). All atoms are at the experimental X-ray geometry, except for methyl groups, allene moiety and hydrogen atoms (see Results section for details). Only densities larger than 0.02 (in absolute value) are reported.

densities are drawn in Fig. 7. The spin density of the triplet localized on peridinin is virtually indistinguishable from that obtained for the isolated peridinin at the same geometry: the Mulliken spin densities computed in this latter case are shown in Fig. 8. A qualitative prediction of large hfcs can be performed on inspection of Fig. 8 remembering that the isotropic hfc constants of hydrogen atoms lying in the nodal plane of π open-shell systems are roughly proportional to the spin density of the carbon atoms to which they are attached (spin polarization mechanism). Thus, we expect large negative hfcs on protons H1, H10, H12, and average negative values on H8 and H9. Positive (but not too large) values are expected, instead, for protons H2, H6, H13, and H15. Of course protons of methyl groups lying out the nodal plane have a direct contribution from singly occupied orbitals and, hence, quite large positive hfcs. Since, however, a single average value is observed for the three protons of each methyl group (due to tunnelling and/or free rotation), the average value is reduced by the vanishing contribution of hydrogen atom(s) lying in the nodal plane.

Table 3 collects the hfcs of the most significant protons: it is apparent that the qualitative expectations are confirmed by explicit computations. The A tensors reported in Table 3 contain both the isotropic and the dipolar contributions. The axes of dipolar couplings are oriented along the ZFS axes as determined experimentally. Note that we have assumed a free rotation of methyl groups, so that the corresponding hfcs are averages over the three protons for four representative values of the C–C–C–H dihedral angle (0°, 30°, 60°, and 90°).

The computed values for methyl groups are in remarkable agreement with the experiment. We can therefore unequivocally assign the large positive hfcs measured in the ZFS axes directions to two sets of equivalent methyl protons: the largest $a_{iso}=10.6$ MHz can be attributed to methyl 19 and $a_{iso}=7.0$ MHz to methyl group 18 (for the molecular positions see Fig. 1B).

Concerning α-protons, small positive hfc tensor components ($A_{XX}\leq 2.7$ MHz, $A_{YY}\leq 1.2$ MHz $A_{ZZ}\leq 2.9$ MHz) and small negative components ($A_{YY}\leq -1.0$ MHz), as determined experimentally, are in agreement with computed values for protons H2, H4, H6, H11, H13 and H15. Large negative hfc components in the *Y* and *Z* directions of the ZFS tensor, as computed for H10 and H12, have not been detected in the ENDOR, likely due to anisotropic broadening of the corresponding lines. The computed $A_{XX}$ components for H10 and H12 are compatible with

Table 3
Proton hyperfine couplings for the peridinin triplet state as derived from DFT calculations

| Position [a] | Computed values [b] | | | |
|---|---|---|---|---|
| | $A_{XX}$ (MHz) | $A_{YY}$ (MHz) | $A_{ZZ}$ (MHz) | $a_{iso}$ (MHz) |
| 1 | −3.59 / −3.3 | −8.24 / −8.04 | −10.28 / −9.66 | −7.37 / −7.00 |
| 2 | 1.34 / 1.38 | 0.44 / 0.71 | 2.66 / 2.93 | 1.48 / 1.67 |
| 4 | 0.89 / 0.53 | −0.95 / −1.61 | 0.74 / −0.33 | 0.23 / −0.47 |
| 6 | −0.04 / −0.48 | −2.72 / −3.74 | −0.66 / −1.96 | −1.14 / −2.06 |
| 8 | −1.14 / −1.5 | −5.35 / −6.4 | −5.07 / −6.38 | −3.85 / −4.76 |
| 9 | −0.87 / −0.73 | −4.81 / −4.95 | −4.79 / −4.79 | −3.49 / −3.49 |
| 10 | −2.45 / −2.71 | −8.09 / −8.85 | −9.77 / −10.6 | −6.77 / −7.39 |
| 11 | 0.58 / 0.58 | −1.86 / −1.94 | 0.44 / 0.25 | −0.28 / −0.37 |
| 12 | −3.97 / −4.06 | −10.64 / −11.12 | −14.63 / −15.06 | −9.75 / −10.08 |
| 13 | 1.45 / 1.46 | −0.04 / 0.18 | 3.42 / 3.58 | 1.61 / 1.74 |
| 15 | 2.16 / 2.26 | 0.8 / 1.04 | 3.58 / 3.54 | 2.18 / 2,28 |
| 18 Me | 7.16 / 7.04 | 5.33 / 5.04 | 6,31 / 6.1 | 6.27 / 6.06 |
| 19 Me | 11,25 / 10.53 | 9.11 / 8.63 | 10.04 / 9.55 | 10.13 / 9.57 |

This table reports the computed values (B3LYP / epr-II) of the proton hyperfine tensor components in the ZFS axes system of the peridinin molecule, as well as the isotropic hyperfine couplings. The ZFS reference frame is reported in Fig. 1B.

[a] See Fig. 1B for molecular positions.

[b] Pairs of values refer to pseudo-symmetric peridinins (Per614 and Per624).

experimental values in the $X$ direction ($A_{XX}=-3.6$ MHz, $A_{XX}=-6.9$ MHz). Computed hfcs of protons H8 and H9 are compatible with negative components measured in the $Y$ and $Z$ directions ($A_{YY}=-4.1$ MHz, $A_{YY}=-6.9$ MHz and $A_{ZZ}=-3.3$ MHz) and with the small negative component in the $X$ direction ($A_{XX}=-0.9$ MHz).

The situation could be more involved for H1, located on the "terminal" part of peridinin, which could experience significant geometry variations upon passage from singlet (to which X-ray geometry refers) to triplet (to which EPR measurements refer) electronic states, and for this reason it has not been considered in the tentative assignment of the ENDOR lines.

## 4. Discussion

As an extension of our previous investigation [13], in the present manuscript we focused our attention on seeking the correlation between the specific Chl601(602)–Per614(624) pair identified by the time-resolved EPR experiments and the structural requirements for efficient triplet energy transfer as indicated by the X-ray structural data [14].

Triplet–triplet energy transfer, based on the Dexter mechanism, depends on stringent overlap requirement between the donor and acceptor wavefunctions and is very sensitive to distance and mutual orientation between the π orbitals of the molecules involved [41]. Small differences in the relative geometry of the donor–acceptor pair are expected to lead to preferential pathways in the triplet quenching. In the PCP complex the X-ray structure has shown the complexity of the system in terms of pigment arrangement: all four peridinins surrounding the Chl *a* molecule are at van der Waals distance with the tetrapyrrole ring but the contact involves different parts of the donor and acceptor conjugated systems. Therefore, the distance requirement is fulfilled for all four carotenoid molecules and other factors based on fine-tuning of the relative geometry of the pair and on the electron density distribution on the extended conjugated systems play the major role. Detailed knowledge of the electronic structure of the triplet state of the molecules involved in the energy transfer is necessary in order to investigate this issue.

We have performed pulse ENDOR experiments on the photoexcited peridinin triplet state in the PCP antenna complex from *A. carterae* in order to access the hyperfine structure information on the photoexcited peridinin triplet state. ENDOR measurements at all canonical orientations where the static magnetic field is parallel to the ZFS tensor axes, allowed us to obtain a partial set of hyperfine tensor values for all three canonical orientations. All the positive hyperfine coupling tensor components, in the ZFS reference frame, corresponding to two different rotating methyl groups have been derived. Some positive and negative hyperfine components belonging to α-protons have also been detected, whose experimental values are in agreement with DFT calculations on the proton hyperfine coupling tensors for the peridinin triplet state. However, some of the large negative hyperfine components, belonging to α-protons, as predicted by DFT calculations (see Table 3), are missing. This problem was already encountered in the ENDOR study of different carotenoid cation radicals both in protein and *in vitro* systems [18,21]. ENDOR lines corresponding to α-protons are broaden because of the large anisotropic component and may become undetectable in powder ENDOR spectra.

Although precise assignment of the whole set of experimental hfcs, based on DFT calculation of the hyperfine tensors, is not possible because of some missing ENDOR lines, unequivocal assignment of the two sets of large positive hyperfine tensor components to the rotating methyl groups at positions 18, 19 of the peridinin conjugated chain allows to draw important conclusions on the electronic structure of the peridinin triplet state.

These two methyl groups have been used as markers of the electronic structure of the triplet state. The satisfactory agreement between the experimental and computed hyperfine couplings assigned to the rotating methyl groups on the conjugated chain, provide a critical test of the triplet state wave function. The calculated spin density on the peridinin triplet state gives an important picture of how the two singly occupied orbitals of the triplet state are distributed over the conjugated chain of the peridinin molecule (see Figs. 7 and 8). DFT calculations show that the unpaired spins are quite delocalized over the whole conjugated system, with an alternate spin pattern with positive spin densities alternating with gradually smaller negative spin densities. This alternate pattern is lost in the central region of the conjugated chain where all positive densities are found. Very similar behaviour was reported for a series of carotenoid radical cations employing B3LYP hybrid density functional theory method [42].

An inspection on distances of closest contact between the conjugated regions of the Chl *a* molecule and each of the surrounding peridinins using the X-ray data information [14], while considering the spin density distribution on the two pigments, opens a new perception of how triplet energy transfer prerequisites are satisfied by Per614(624) more than any other peridinin in the PCP complex. For this reason we have computed the spin density distribution over the conjugated system for both the peridinin triplet state and for the Chl *a* triplet state. Considering distances short enough to ensure triplet energy transfer (<5 Å) [43] and molecular positions with significant spin densities, the closest approach between the donor and acceptor molecules involves different portions of the two conjugated systems. While for Per614(624) the central region of the polyene conjugated chain is in close contact to the chlorophyll, for the other peridinins the terminal portion of the polyene chain including the allene moiety is approaching the tetrapyrrole ring to variable extent. However, experimental and computed hfcs prove that the triplet spin density is distributed in an uniform alternate pattern all over the polyene conjugated chain, and this difference is not important in terms of triplet energy transfer requirements. On the other hand, Per611(621) and Per613(623) have only point-like contacts with the tetrapyrrole ring of the Chl *a* donor, while both Per612(622) and Per614(624) overlap with an extended region of the macrocycle, which includes, at least partially, two pyrrole rings characterized by significant contributions of spin density. The major fact which seems to prevent the required overlap between the

donor and acceptor molecules in the case of Per611(621) and Per613(623) is the absence of an extended contact with high densitiy regions of the Chl *a* macrocycle rather than the overlap with different regions of the peridinin conjugated chain. Even though no evidence has come out from this inspection based on distance and spin densities requirements, the involvement of Per612(622) in photoprotection was already excluded on the basis of time-resolved experiments on the high-salt PCP [13], a minor component of PCP whose cluster is lacking Per2 [44].

Further insight into the triplet spin density distribution on the π-conjugated system of the peridinin molecule reveals that the second highest spin density value is found at the carbon position (C12 in Fig. 1) of closest approach to the water molecule which is coordinated to the central Mg atom of Chl *a* and placed at the interface between the Chl601(602)–Per614(624) pair. This result reinforces the hypothesis, already proposed in [13], that the water ligand may play the role of extending the overlap between Chl *a* and Per614(624), acting as a bridge in the triplet–triplet energy transfer between the two pigments.

Triplet energy transfer, via the Dexter mechanism, depends on stringent overlap requirements between the donor and acceptor wave functions. Involvement of a molecular bridge between donor and acceptor molecules, which can mediate electron exchange, may become important for efficient and competitive transfer among pigments, especially for the expected small vacuum couplings between the couple involved in the transfer [45,46].

The interfacial water molecule is an unique feature of Per614 (624) since no bridging amino acid or water molecule is present at the interface between Chl *a* and the other peridinins. The high spin densities at the carbon position of the conjugated chain with the minimum distance to the bridging water reinforces the concept of exclusive involvement of Per614(624) in the photoprotective mechanism.

As a further step in the investigation, the ENDOR experiments were performed at different temperatures (5 K–150 K) and various delay times between the laser flash, used to photoexcite the triplet species, and the pulse ENDOR sequence. This wide set of ENDOR data was employed to further prove the triplet localization concept introduced in our previous manuscript [13].

No temperature effect, in the range of experimental observation, has been observed in the ENDOR spectra detected at the ZFS canonical orientations. If triplet hopping among peridinins in the cluster is already active at cryogenic temperatures, it is then occurring too fast to influence ENDOR line positions. An argument against fast hopping is that a reduction of hfcs should have been detected while experimental and computed values for a localized triplet state on a single peridinin molecule are in good agreement. Furthermore, no evidence of thermally activated hopping was produced by time-resolved experiments performed on the PCP cluster in a wide temperature range from cryogenic to physiological temperatures [13].

Recently, a delocalized triplet model, in which the carotenoid triplet state is delocalized over the adjacent Chl *a* molecule leading to the mixing of Chl triplet character in the peridinin triplet state, has been proposed by Alexandre et al. to interpret step-scan Fourier transform infrared spectroscopy data obtained for PCP in *A. carterae* [47]. No indication is coming from the ENDOR experiments and DFT calculations of any peridinin–Chl *a* delocalization in the triplet state. Considering the chlorophyll–peridinin pair, we found two low-lying triplet states localized respectively on the chlorophyll and on the peridinin molecules. The spin density of the triplet state localized on the peridinin molecule in the pair is virtually indistinguishable from that obtained for the isolated peridinin molecule in the same geometry.

Detection of ENDOR spectra at different delay times from the laser flash allowed to follow the time-evolution of the peridinin triplet state while probing the hyperfine coupling observable, which should be a very sensitive probe of conformational changes of the polyene conjugated chain. Any triplet migration to other peridinin molecules in the cluster would have been detected in terms of line shifts in the ENDOR spectra recorded at longer DAF. Such effects are predicted by DFT calculations of the triplet hyperfine couplings for each peridinin of the cluster in the corresponding X-ray geometry (data not shown). The crystal structure indicates that the eight peridinin binding sites are not equivalent with respect to carotenoid geometry [14]. In particular, variations of the order of 1–2 MHz have been computed for the isotropic hyperfine constants of the two rotating methyl groups for the eight peridinins. On the contrary, the ENDOR spectra at different delays are superimposable proving that the triplet state is localized on the same peridinin molecule during the overall triplet lifetime. The evolution in time of the ESP of the peridinin triplet including the spin polarization inversion detected at the *Y* canonical transitions, which is not accompanied by any ENDOR spectral variation, is due, as proved by simulations, to the strongly anisotropic decay of the three spin sublevels of the peridinin triplet state to the ground state. No triplet–triplet migration to a neighbour peridinin or conformational readjustment of the carotenoid triplet state need to be invoked to explain the time-dependence of the ESE spectra.

As a concluding remark, the combined use of pulse EPR and ENDOR spectroscopies and theoretical methodologies has provided detailed information on the electronic structure of the excited triplet state of the peridinin carotenoid in the PCP antenna from *A. carterae*, strongly supporting the hypothesis of localization of the triplet state on one specific peridinin. High spin density has been found particularly at the carbon atom position, which for the peridinin involved in the photoprotective mechanism is in close contact with the water ligand to the Chl *a* pigment. This result reinforces the hypothesis, already proposed in [13], that the water ligand is functioning has a super-exchange bridge in the triplet–triplet energy transfer between the Chl *a* donor and the peridinin acceptor in the PCP antenna.

## 5. Note

After submission of this manuscript a communication on a Q-band pulse ENDOR and DFT study on the peridinin triplet

state was published [48]. While our investigation is on the native PCP from *A. carterae*, in this study the antenna complex under investigation is the refolded N-domain PCP, expressed in *Escherichia coli*. Dimerization of the N-domain occurs upon refolding to form a PCP similar to that from the dinoflagellate species *Heterocapsa*. A comparison between our ENDOR/DFT data results on the native protein and those on the refolded N-domain PCP shows that there are no significant differences in the hyperfine couplings of the peridinin triplet state in the two complexes. Localization of the triplet on one specific peridinin proposed by our group, based on the time-resolved [13] and ENDOR investigations, is found also in the refolded N-domain PCP.

## Acknowledgements

This work was supported by the Italian Ministry for University and Research (MURST) under the project PRIN2005, and by NSF (MCB-9983034 to A.A.). We thank Prof. Giovanni Giacometti for fruitful discussions and advice.

## References

[1] H.A. Frank, R.J. Cogdell, Carotenoids in photosynthesis, Photochem. Photobiol. 63 (1996) 257–264.
[2] W.J. McGann, H.A. Franck, Transient electron spin resonance spectroscopy of the carotenoid triplet state in *Rhodopseudomonas sphaeroides* wild type, Chem. Phys. Lett. 121 (1985) 253–261.
[3] I.V. Borovykh, I.B. Klenina, I.I. Proskuryakov, P. Gast, A.J. Hoff, Magnetophotoselection study of the carotenoid triplet state in *Rhodobacter sphaeroides* reaction centers, J. Phys. Chem. B 106 (2002) 4305–4312.
[4] Y. Kakitani, R. Fujii, Y. Koyama, H. Nagae, L. Walker, B. Salter, A. Angerhofer, Triplet-state conformational changes in 15-*cis*-spheroidene bound to the reaction center from *Rhodobacter sphaeroides* 2.4.1 as revealed by time-resolved EPR spectroscopy: strengthened hypothetical mechanism of triplet-energy dissipation, Biochemistry 45 (2006) 2053–2062.
[5] D. Carbonera, M. Di Valentin, G. Agostini, G. Giacometti, P.A. Liddell, D. Gust, A.L. Moore, T.A. Moore, Energy transfer and spin polarization of the carotenoid triplet state in synthetic carotenoporphyrin dyads and in natural antenna complexes, Appl. Magn. Reson. 13 (1997) 487–504.
[6] R. Bittl, E. Schlodder, I. Geisenheimer, W. Lubitz, R.J. Cogdell, Transient EPR and absorption studies of carotenoid triplet formation in purple bacterial antenna complexes, J. Phys. Chem. B 105 (2001) 5525–5535.
[7] D. Carbonera, M. diValentin, C. Corvaja, G. Giacometti, G. Agostini, P.A. Liddell, A.L. Moore, T.A. Moore, D. Gust, Carotenoid triplet detection by time-resolved EPR spectroscopy in carotenopyropheophorbide dyads, J. Photochem. Photobiol., A Chem. 105 (1997) 329–335.
[8] M. Di Valentin, A. Bisol, G. Agostini, M. Fuhs, P.A. Liddell, A.L. Moore, T.A. Moore, D. Gust, D. Carbonera, Photochemistry of artificial photosynthetic reaction centers in liquid crystals probed by multifrequency EPR (9.5 and 95 GHz), J. Am. Chem. Soc. 126 (2004) 17074–17086.
[9] M. Di Valentin, A. Bisol, G. Agostini, G. Giacometti, D. Carbonera, EPR-detected photoinduced electron transfer in three structurally related molecular triads, Appl. Magn. Reson. 30 (2006) 555–576.
[10] M.A. El-Sayed, D.E. Tinti, E.M. Yee, Conservation of spin direction and production of spin alignment in triplet–triplet energy transfer, J. Chem. Phys. 51 (1969) 5721–5723.
[11] K. Akiyama, S. Terokubota, T. Ikoma, Y. Ikegami, Spin polarization conservation during intramolecular triplet-triplet energy-transfer studied by time-resolved EPR spectroscopy, J. Am. Chem. Soc. 116 (1994) 5324–5327.
[12] R. Fujii, K. Furuichi, J.P. Zhang, H. Nagae, H. Hashimoto, Y. Koyama, *Cis*-to-*trans* isomerization of spheroidene in the triplet state as detected by time-resolved absorption spectroscopy, J. Phys. Chem. A 106 (2002) 2410–2421.
[13] M. Di Valentin, S. Ceola, E. Salvadori, G. Agostini, D. Carbonera, Identification by Time-Resolved EPR of the peridinins directly involved in chlorophyll triplet quenching in the Peridinin - Chlorophyll *a* - Protein from *Amphidinium carterae*, Biochim. Biophys. Acta 1777 (2008) 186–195.
[14] E. Hofmann, P.M. Wrench, F.P. Sharples, R.G. Hiller, W. Welte, K. Diederichs, Structural basis of light harvesting by carotenoids: peridinin-chlorophyll-protein from *Amphidinium carterae*, Science 272 (1996) 1788–1791.
[15] J.A. Bautista, R.G. Hiller, F.P. Sharples, D. Gosztola, M. Wasielewski, H.A. Frank, Singlet and triplet energy transfer in the peridinin - chlorophyll *a* - protein from *Amphidinium carterae*, J. Phys. Chem. A 103 (1999) 2267–2273.
[16] G.L. Closs, P. Piotrowiak, J.M. MacInnis, G.R. Fleming, Determination of long distance intramolecular triplet energy transfer rates. A quantitative comparison with electron transfer, J. Am. Chem. Soc. 110 (1988) 2652–2653.
[17] G.L. Closs, M.D. Johnson, J.R. Miller, P. Piotrowiak, A connection between intramolecular long-range electron, hole and triplet energy transfer, J. Am. Chem. Soc. 11 (1989) 3751–3753.
[18] P. Faller, T. Maly, A.W. Rutherford, F. MacMillan, Chlorophyll and carotenoid radicals in photosystem II studied by pulsed ENDOR, Biochemistry 40 (2001) 320–326.
[19] L. Piekara-Sady, M.M. Khaled, E. Bradford, L.D. Kispert, M. Plato, Comparison of the Indo to the Rhf-Indo/Sp derived EPR proton hyperfine couplings for the carotenoid cation radical — experimental-evidence, Chem. Phys. Lett. 186 (1991) 143–148.
[20] L. Piekara-Sady, A.S. Jeevarajan, L.D. Kispert, An ENDOR study of the canthaxanthin cation-radical in solution, Chem. Phys. Lett. 207 (1993) 173–177.
[21] T.A. Konovalova, S.A. Dikanov, M.K. Bowman, L.D. Kispert, Detection of anisotropic hyperfine components of chemically prepared carotenoid radical cations: 1D and 2D ESEEM and pulsed ENDOR study, J. Phys. Chem. B 105 (2001) 8361–8368.
[22] C.W.M. Kay, M. Divalentin, K. Mobius, A time-resolved electron-nuclear double-resonance (ENDOR) study of the photoexcited triplet-state of free-base tetraphenylporphyrin, Sol. Energy Mater. Sol. Cells 38 (1995) 111–118.
[23] C.W.M. Kay, M. Di Valentin, K. Mobius, Time-resolved EPR and ENDOR study of the photoexcited triplet state of free-base tetraphenylchlorin in a crystalline toluene matrix, J. Chem. Soc., Perkin Trans. 2 (1997) 2563–2568.
[24] C.W.M. Kay, U. Gromadecki, J.T. Torring, S. Weber, An investigation of the structure of free-base porphycene by time-resolved electron nuclear double resonance and density functional theory on the photoexcited triplet state, Mol. Phys. 99 (2001) 1413–1420.
[25] M. DiValentin, C.W.M. Kay, G. Giacometti, K. Mobius, A time-resolved electron nuclear double resonance study of the photoexcited triplet state of P680 in isolated reaction centers of photosystem II, Chem. Phys. Lett. 248 (1996) 434–441.
[26] F. Lendzian, R. Bittl, A. Telfer, W. Lubitz, Hyperfine structure of the photoexcited triplet state $^3$P680 in plant PSII reaction centres as determined by pulse ENDOR spectroscopy, Biochim. Biophys. Acta 1605 (2003) 35–46.
[27] F. Lendzian, R. Bittl, W. Lubitz, Pulsed ENDOR of the photoexcited triplet states of bacteriochlorophyll a and of the primary donor $P_{865}$ in reaction centers of *Rhodobacter sphaeroides* R-26, Photosynth. Res. 55 (1998) 189–197.
[28] S. Parrish, A. Angerhofer. (1999), pp. 22–23, NHFML, Talahasse, Florida.
[29] F.P. Sharples, P.M. Wrench, K.L. Ou, R.G. Hiller, Two distinct forms of the peridinin-chlorophyll alpha-protein from *Amphidinium carterae*, Biochim. Biophys. Acta 1276 (1996) 117–123.
[30] T.-S. Lin, Electron spin echo spectroscopy of organic triplets, Chem. Rev. 84 (1984) 1–15.
[31] M.J. Frisch, G.W. Truks, H.B. Schlegel, G.E. Scuseria, M.A. Robb, J.R. Cheeseman, J. Montgomery, J.A., T. Vreven, K.N. Kudin, J.C. Burant, J.M. Millam, S.S. Iyengar, J. Tomasi, V. Barone, B. Mennucci, M. Cossi, G.

Scalmani, N. Rega, G.A. Petersson, H. Nakatsuji, M. Hada, M. Ehara, K. Toyota, R. Fukuda, J. Hasegawa, M. Ishida, T. Nakajima, Y. Honda, O. Kitao, H. Nakai, M. Klene, X. Li, J.E. Knox, H.P. Hratchian, J.B. Cross, V. Bakken, C. Adamo, J. Jaramillo, R. Gomperts, R.E. Stratmann, O. Yazyev, A.J. Austin, R. Cammi, C. Pomelli, J.W. Ochterski, P.Y. Ayala, K. Morokuma, G.A. Voth, P. Salvador, J.J. Dannenberg, V.G. Zakrzewski, S. Dapprich, A.D. Daniels, M.C. Strain, O. Farkas, D.K. Malick, A.D. Rabuck, K. Raghavachari, J.B. Foresman, J.V. Ortiz, Q. Cui, A.G. Baboul, S. Clifford, J. Cioslowski, B.B. Stefanov, G. Liu, A. Liashenko, P. Piskorz, I. Komaromi, R.L. Martin, D.J. Fox, T. Keith, M.A. Al-Laham, C.Y. Peng, A. Nanayakkara, M. Challacombe, P.M.W. Gill, B. Johnson, W. Chen, M.W. Wong, C. Gonzalez, J.A. Pople, Revison D.02 ed. Gaussian, Inc., Wallingford, CT, 2004.

[32] J.B. Foresman, A.E. Frisch, Exploring Chemistry with Electronic Structure Methods, Gaussian Inc., Pittsburg, PA, 1996.

[33] V. Barone, Characterization of the potential-energy surface of the $HO_2$ molecular-system by a density-functional approach, J. Chem. Phys. 101 (1994) 10666–10676.

[34] V. Barone, Inclusion of Hartree-Fock exchange in density-functional methods — hyperfine-structure of 2nd row atoms and hydrides, J. Chem. Phys. 101 (1994) 6834–6838.

[35] J. Frick, J.U. Vonschutz, H.C. Wolf, G. Kothe, 1st detection of the (nonphosphorescent) triplet-state in single-crystals of beta-carotene, Mol. Cryst. Liq. Cryst. 183 (1990) 269–272.

[36] J. Frick, PhD Thesis, Stuttgart, 1992.

[37] A. Schweiger, G. Jeschke, Principles of Pulse Paramagnetic Resonance, Oxford University Press, Oxford, 2001.

[38] A. Carrington, A.D. McLachlan, Introduction to Magnetic Resonance: With Applications to Chemistry and Chemical Physics, Chapman and Hall, London, 1979.

[39] D. Carbonera, G. Giacometti, U. Segre, A. Angerhofer, U. Gross, Model for triplet–triplet energy transfer in natural clusters of peridinin molecules contained in dinoflagellate's outer antenna proteins, J. Phys. Chem. B 103 (1999) 6357–6362.

[40] R. Improta, V. Barone, Interplay of electronic, environmental, and vibrational effects in determining the hyperfine coupling constants of organic free radicals, Chem. Rev. 104 (2004) 1231–1253.

[41] D.L. Dexter, A theory of sensitized luminescence in solids, J. Chem. Phys. 21 (1953) 836–850.

[42] J.D. Guo, Y. Luo, F. Himo, Density functional theory study of the canthaxanthin and other carotenoid radical cations, Chem. Phys. Lett. 366 (2002) 73–81.

[43] Z.Q. You, C.P. Hsu, G.R. Fleming, Triplet–triplet energy-transfer coupling: theory and calculation, J. Chem. Phys. 124 (2006).

[44] R.P. Ilagan, J.F. Koscielecki, R.G. Hiller, F.P. Sharples, G.N. Gibson, R.R. Birge, H.A. Frank, Femtosecond time-resolved absorption spectroscopy of main-form and high-salt peridinin - chlorophyll *a* - proteins at low temperatures, Biochemistry 45 (2006) 14052–14063.

[45] H.B. Gray, J.R. Winkler, Electron transfer in chemistry, 2001.

[46] J.P. Lin, I.A. Balabin, D.N. Beratan, The nature of aqueous tunneling pathways between electron-transfer proteins, Science 310 (2005) 1311–1313.

[47] M.T.A. Alexandre, D.C. Luhrs, I.H.M. van Stokkum, R. Hiller, M.L. Groot, J.T.M. Kennis, R. Van Grondelle, Triplet state dynamics in peridinin – chlorophyll *a* – protein: a new pathway of photoprotection in LHCs? Biophys. J. 93 (2007) 2118–2128.

[48] J. Niklas, T. Schulte, S. Prakash, M. van Gastel, E. Hofmann, W. Lubitz, Spin density distribution of the carotenoid triplet state in the peridinin–chlorophyll–protein antenna. A Q-band pulse ENDOR and DFT study, J. Am. Chem. Soc. 129 (2007) 15442–15443.